Supplementary Material for: "Attosecond probing and control of charge migration in carbon-chain molecule"

Lixin He[a], Yanqing He[a], Siqi Sun[a], E. Goetz[c], Anh-Thu Le[c], Xiaosong Zhu[a], Pengfei Lan[a,*], Peixiang Lu[a,b,†], C. D. Lin[d]

[a]Wuhan National Laboratory for Optoelectronics and School of Physics, Huazhong University of Science and Technology, Wuhan 430074, China

[b]Hubei Key Laboratory of Optical Information and Pattern Recognition, Wuhan Institute of Technology, Wuhan 430205, China

[c]Department of Physics, University of Connecticut, Storrs, CT 06269-3046, USA

[d]Department of Physics, Kansas State University, Manhattan, KS 66506, USA

1. Experimental details

Our experimental setup is sketched in Fig. S1. The output of a commercial Ti: sapphire laser system (Astrella-USP-1K, Coherent, Inc.), which delivers 35 fs, 800 nm laser pulses at a repetition rate of 1 kHz, is split into two beams by a beam splitter (BS) for the nonadiabatic alignment of C_4H_2 molecules (the aligning laser, P_1) and the generation of harmonics (the driving laser, P_2). The aligning and driving pulses are parallel in the polarization. The time delay between these two pulses is adjusted by a motorized delay line installed in the arm of the aligning pulse. These two pulses are collinearly focused into a supersonic gas jet ejected from a nozzle (250 μm diameter) with a backing pressure of 0.2 bars by a spherical mirror (f=250 mm). The gas jet is placed 2 mm after the laser focus to ensure good phase matching of the short-trajectory harmonics. The generated high harmonics are detected by a homemade flat-field soft x-ray spectrometer,[55] which includes a 0.1-mm-wide, 15-mm-height entrance slit, a flat-field grating (1200 grooves mm^{-1}), and a microchannel plate (MCP) backed with a phosphor screen. A charge-coupled device (CCD) camera is used to record the harmonic spectral images.

In our experiment, we first measured HHG from C_4H_2 by using a one-color driving field. In this case, the driving laser P_2 is directly used to generate high-order harmonics. Figure S2 shows

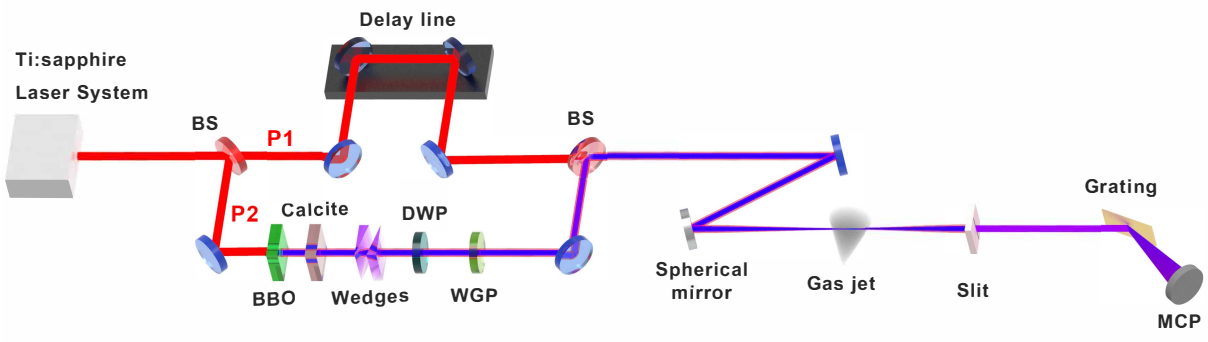

Fig S1 Schematic diagram of the experimental set-up. BS: beam splitter, DWP: dual-wave plate, WGP: wire grid polarizer, MCP: microchannel plate.

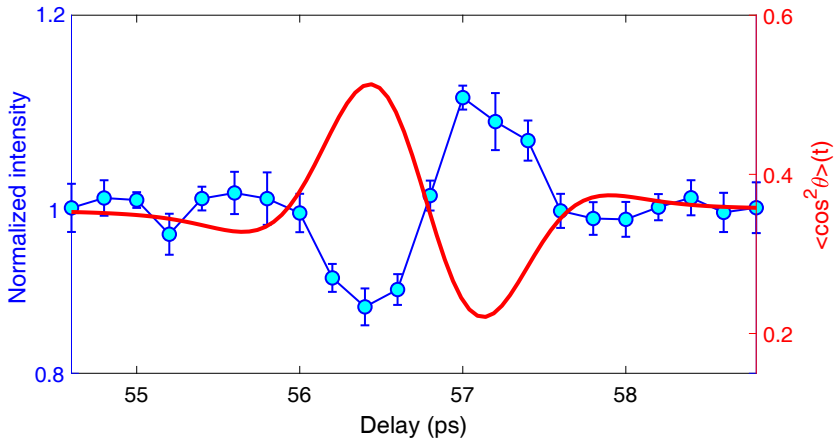

Fig S2 HHG signals (circles) of H13 measured around the half-rotational revival of C_4H_2 in the one-color driving laser field. Error bars represent the standard deviations of nine independent measurements. The red line shows the time-dependent degrees of molecular alignment $\langle\cos^2\theta\rangle$(t) retrieved from the experimental data of H13.

the delay-dependent signals (solid line with circles) of the 13th harmonic (H13) measured around the half-rotational revival of C_4H_2 molecule. The one-color result has been used to determine the alignment distribution of the molecules in our experiment with the method outlined in.[44] The red line in Fig. S2 plots the retrieved time-dependent alignment parameter $\langle\cos^2\theta\rangle$(t). The degree of alignment in our experiment is about 0.5 ($\langle\cos^2\theta\rangle_{max}$). It is a typical level of molecular alignment in experiments.

On the other hand, to extract the CM dynamics, multiple experimental observables are required to decompose the multichannel contributions. In our experiment, we adopt a parallel two-color driving scheme. As shown in Fig. S1, a type-I BBO crystal is installed in the arm of P_2 to produce

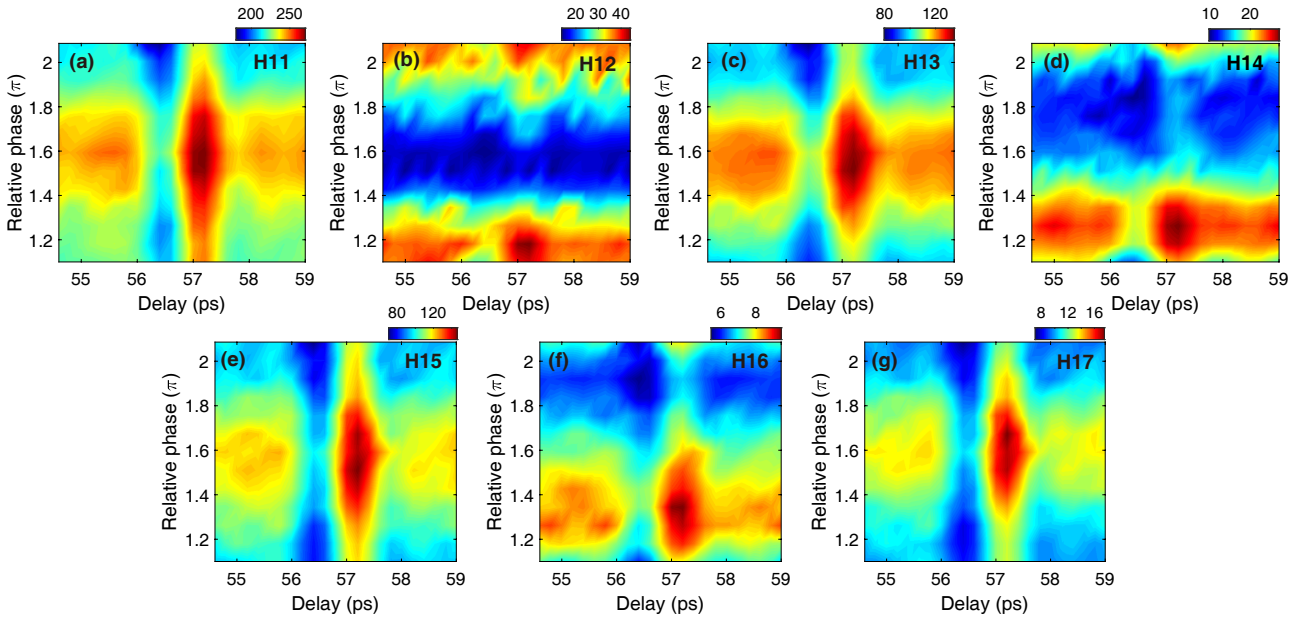

Fig S3 HHG signals of H11-H17 measured around the half-rotational revival of C_4H_2 as a function of the relative phase of the two-color driving field.

a second harmonic (SH) field of the 800 nm fundamental laser. A calcite plate is set to compensate the group-velocity dispersion between the SH and fundamental fields. The relative phase between the SH and fundamental fields is controlled by a pair of wedges. A wire grid polarizer (WGP) is used to ensure the same polarizations of the SH and fundamental fields. The relative intensity between the SH and the fundamental fields is controlled by the combination of a dual-wave plate (DWP, a half wavelength plate at 800 nm and full wavelength plate at 400 nm) and the WGP. In our two-color experiment, the 800 nm laser intensity has been estimated from the harmonic cutoff, which is about 0.95×10^{14} W/cm^2. The intensity of the SH field is about 2×10^{-3} of the fundamental field. In Figs. S3(a)-(b), we plot the HHG signals of both the even and odd harmonics (H11-H17) measured around the half alignment revival of C_4H_2 in the two-color laser field. One can see that the measured HHG signals depend sensitively on the relative phase of the two-color field, and different harmonic orders present different dependencies. Considering the negligible influence of the SH field on the electron dynamics (see below), the measurements in the two-color field thus

can replenish the data set required for the decomposition of the multichannel contributions.

2. Reconstruction method

In the experiment, HHG from the partially aligned molecular ensemble can be expressed as a coherent superposition of the individual radiation weighted by the angular distribution of the molecules,[45–47] i.e.,

$$S(\omega,\tau) = \left| \int_0^{\pi} D(\omega,\theta)\rho(\theta,\tau)sin\theta d\theta \right|^2, \tag{S1}$$

where θ is the alignment angle of the molecule, τ is the time delay between the alignment and driving pulses, $D(\omega,\theta)$ is single-molecule harmonic dipole moment, and $\rho(\theta,\tau)$ is the angular distribution of molecules at delay τ. Since the coherent average over molecular alignment distribution could severely deviate the measurement from the real single molecule response, especially for a low degree of molecular alignment, it is critical to decode the fixed-in-space single-molecule dipole moment $D(\omega,\theta)$ from the measured harmonic signals. In this work, the complex deconvolution was resolved with a recently developed ML algorithm,[36] of which the accuracy and robustness have been verified in both theory and experiment.

By implementing the ML algorithm onto the two-color measurements, we obtained the single-molecule dipole moment $D(\omega,\theta)$ for each relative phase φ of the two-color field. Since the SH field used in our two-color experiment is weak enough and hardly alters the electron dynamics in the molecular ion, that means the complex mixing coefficients $C_{ij}(\theta)$ can be assumed to be independent of the relative phase φ, then we can get

$$D(\omega,\theta;\varphi) = \sum_{i,j=X,A} C_{ij}(\theta) d_{ij}(\omega,\theta;\varphi). \tag{S2}$$

The complex mixing coefficients $C_{ij}(\theta)$ then can be obtained by solving Eq. (S2) with the genetic algorithm. With $C_{ij}(\theta)$ retrieved, we can obtain the complex amplitude of each orbital by,[26,27]

$$P_j(\theta) = \sum_i C_{ij}(\theta)\gamma_i(\theta), \tag{S3}$$

where $\gamma_i(\theta)$ is the initial population of the state i, which is associated with the ionization rate $\eta_i(\theta)$ of each orbital by $|\gamma_i(\theta)|^2 = \eta_i(\theta)/\sum_i \eta_i(\theta)$. Here, the ionization rates $\eta_i(\theta)$ of different molecular orbitals are calculated with the MO-ADK theory.[56–58] The wavefunction of the molecular ion at the recombination instant of each harmonic order then can be obtained by[26,27]

$$\Psi_{sum} = \sum_j P_j(\theta)\Psi_j. \tag{S4}$$

By repeating the above procedure for different harmonic orders, we can ultimately construct the hole dynamics in the ionized molecular ion according to time-frequency mapping underlying HHG.

3. Influence of the SH field on the electron dynamics

To examine the influence of the SH field in our two-color driving scheme on the induced electron dynamics in the C_4H_2 molecule, we have performed three-dimensional simulations based on the time-dependent density functional theory (TDDFT). In our simulations, the two-color fields are expressed as $E(t) = E_1\cos(\omega t) + E_2\cos(2\omega t + \varphi)$, where E_1 and E_2 are the laser intensities of the two-color fields taken from the experiment, and φ is the two-color relative phase. We have performed two-color simulations for the parallel alignment of the C_4H_2 molecule, since in this case, the influence of the external laser field on the electron dynamics is prominent. Figure S4(a) shows the time-dependent population amplitudes ($|P_X|$) of $\tilde{X}$ state of $C_4H_2^+$ ion calculated with

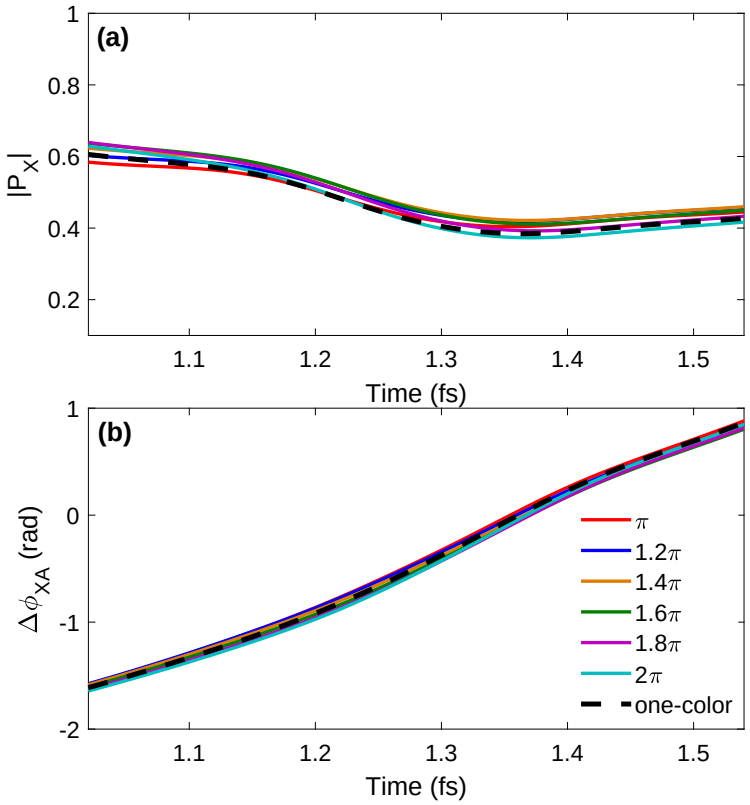

Fig S4 (a) TDDFT calculations of the time-dependent population amplitudes of the $\tilde{X}$ state of $C_4H_2^+$ ion for different relative phases of the two-color laser fields (solid lines). The dashed line shows the result calculated with the fundamental pulse alone for comparison. (b) Same as (a), but for the relative phase between the wave functions of $\tilde{X}$ and $\tilde{A}$ states of the $C_4H_2^+$ ion.

different relative phases of the two-color laser field (solid lines). Figure S4(b) is the corresponding relative phases $\Delta\phi_{XA}$ between the wave functions of $\tilde{X}$ and $\tilde{A}$ states. For comparison, the results calculated with the 800 nm fundamental pulse alone are also presented as the dashed lines. It's obvious that the results (both $|P_X|$ and $\Delta\phi_{XA}$) calculated in the two-color field for different relative phases are very close to that calculated with the fundamental pulse alone, indicating the negligible influence of the weak SH field on the electron dynamics.

4. Alignment-angle-resolved CM in $C_4H_2^+$

In our reconstruction, the harmonic dipoles (both amplitude and phase) for all alignment angles of each fixed-in-space molecule are retrieved from the measured harmonic spectra. Thus, the

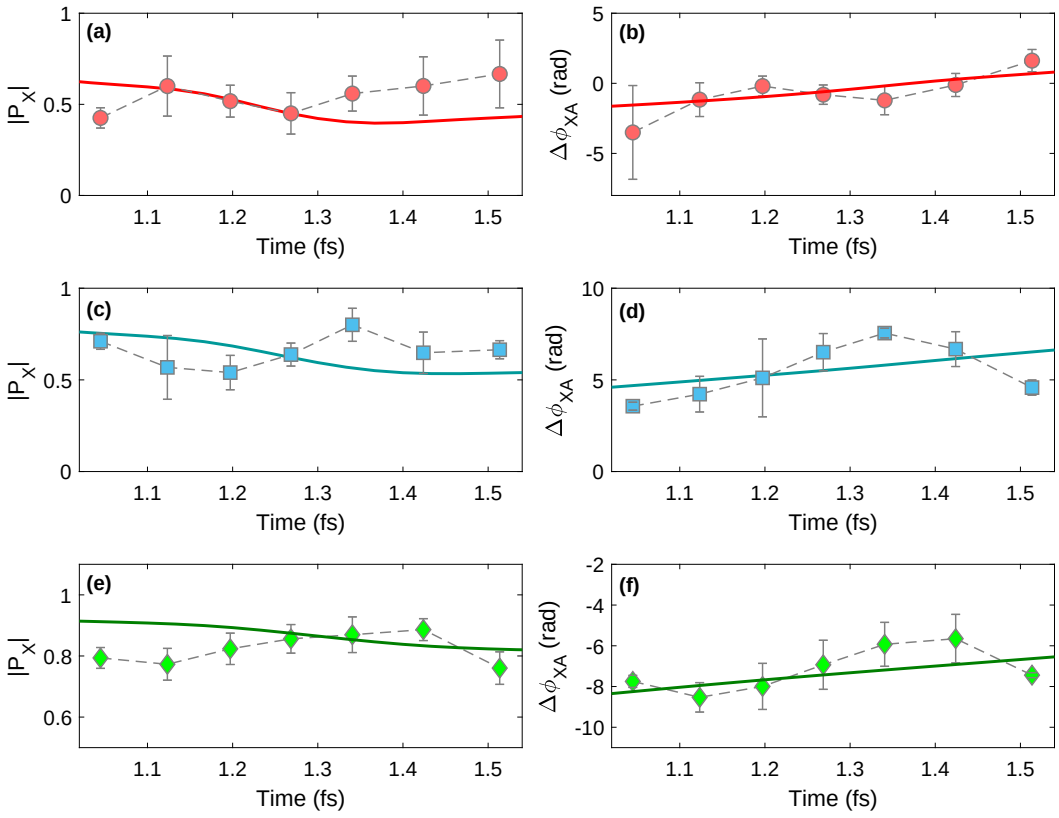

Fig S5 (a)-(b) Retrieved population amplitude of the $\tilde{X}$ state (a) and the relative phase between the wavefunctions of $\tilde{X}$ and $\tilde{A}$ states (b) in C_4H_2 for the alignment angle of 15°. Solid lines in (a)-(b) show the corresponding TDDFT results for comparison. (c)-(d), (e)-(f) Same as (a)-(b), but for the alignment angles of 45° and 75°, respectively.

alignment-angle-dependent CM in the molecule can be fully resolved in our reconstruction. In this section, we discuss the alignment dependence of the CM dynamics in the C_4H_2 molecule. Figure S5 shows the population amplitude of the $\tilde{X}$ state (left column) and the relative phase between the wavefunctions of $\tilde{X}$ and $\tilde{A}$ states (right column) retrieved from the experimental data of H11-H17 for three alignment angles of 15° [(a)-(b)], 45°[(c)-(d)] and 75° [(e)-(f)], respectively. For comparison, the TDDFT simulations of these parameters are also presented as the solid lines in each panel. One can see that the retrievals are in reasonable agreement with the simulations. With these parameters, we have constructed the hole dynamics for these three alignment angles. As shown in Fig. S6, the hole dynamics undergoes significant change as the alignment angle varies.

We have also calculated the reduced hole densities $\rho_x(t)$ for these three angles. The results

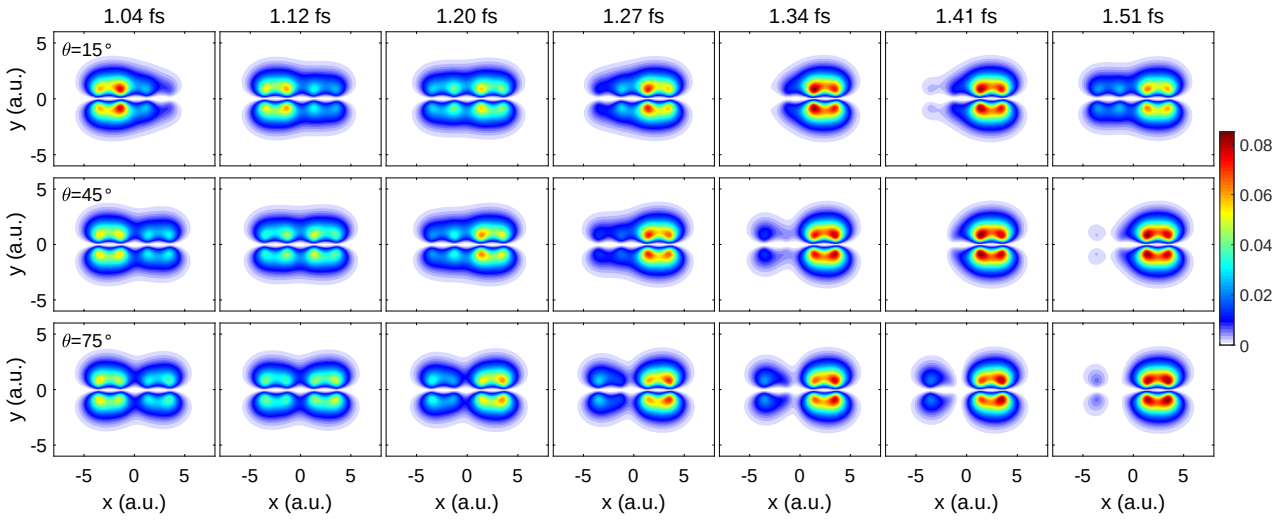

Fig S6 Snapshots of the reconstructed hole densities for the alignment angles of 15° (top row), 45° (middle row) and 75° (bottom row), respectively.

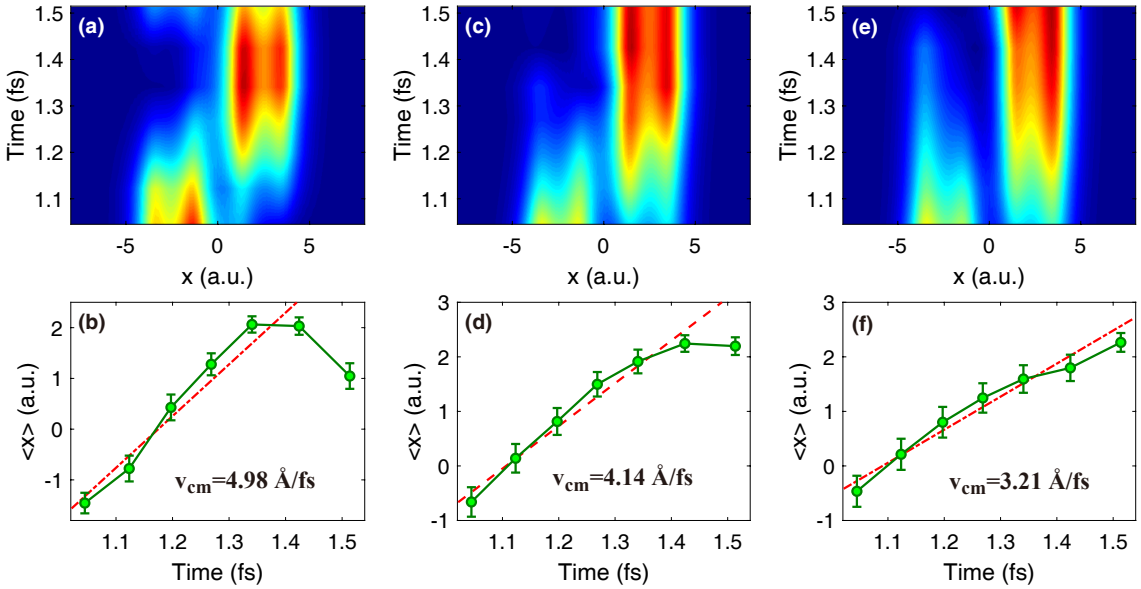

Fig S7 (a) The reduced hole density $\rho_x(t)$ retrieved for the alignment angle of 15°. (b) Time-dependent expected values of the x-coordinate $\langle x\rangle(t)$ (solid line with circles) calculated from the hole densities in (a). The dashed line is a linear fitting of $\langle x\rangle(t)$ to evaluate the CM speed. (c)-(d), (e)-(f) Same as (a)-(b), but for the alignment angles of 45° and 75°, respectively.

are plotted in Figs. S7(a), (c), and (e), respectively. The extracted time-dependent COC positions $\langle x\rangle(t)$ for these three cases are shown as the solid lines with circles in Figs. S7(b), (d), and (f), from which the CM speeds are extracted to be 4.98 Å/fs, 4.14 Å/fs, and 3.21 Å/fs, respectively. A plot of the alignment-angle-dependent CM speeds has been given in the main text (see squares

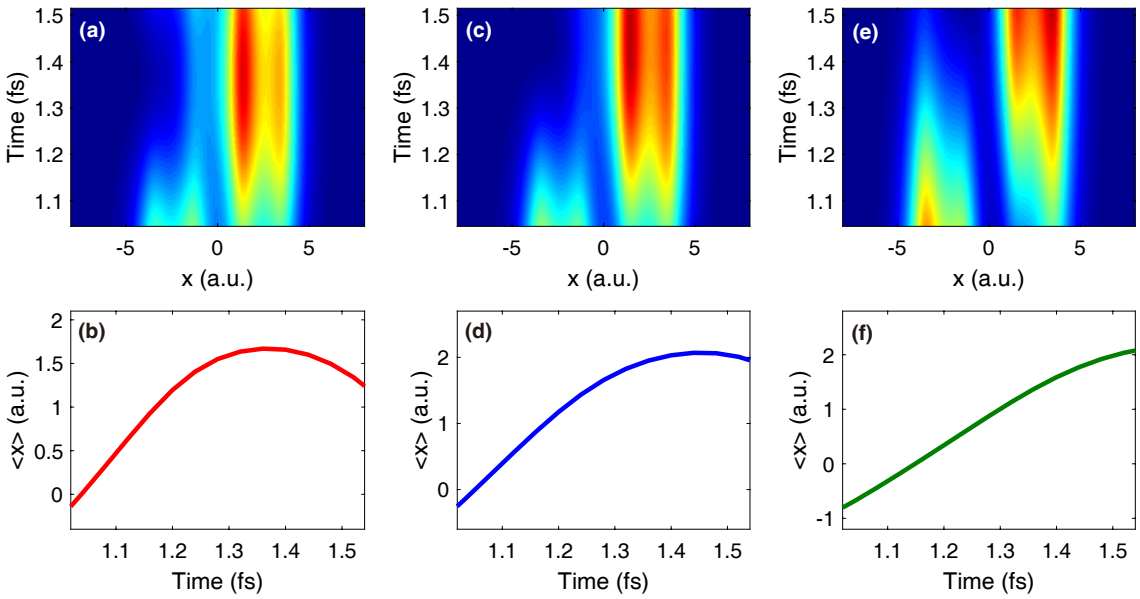

Fig S8 (a) TDDFT simulations of the reduced hole density $\rho_x(t)$ for the alignment angle of 15°. (b) Time-dependent expected values of the x-coordinate $\langle x \rangle(t)$ (solid line with circles) calculated from the hole densities in (a). (c)-(d), (e)-(f) Same as (a)-(b), but for the alignment angles of 45° and 75°, respectively.

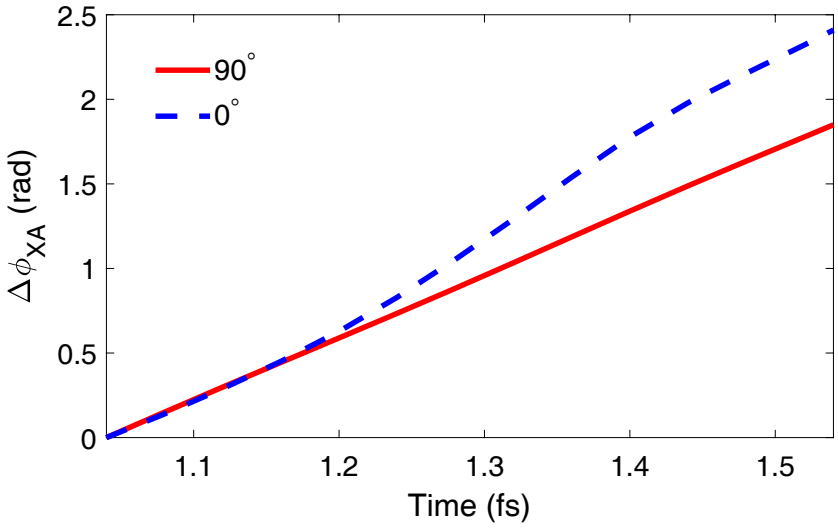

Fig S9 TDDFT simulations of the temporal evolution of the relative phase $\Delta\phi_{XA}$ between the wavefunctions of $\tilde{X}$ and $\tilde{A}$ states for the 90° (red solid line) and 0° (blue dashed line) alignments. For better comparison, the relative phases for these two cases at 1.04 fs have been set to 0.

in Fig. 5). For comparison, we have also performed TDDFT simulations for these three angles. Corresponding results are also displayed in Fig. S8. By comparing Fig. S8 with Fig. S7, one can see good agreement between the experimental reconstructions and the theoretical simulations.

To understand the increase of the CM speed at 0° alignment, we have plotted the TDDFT

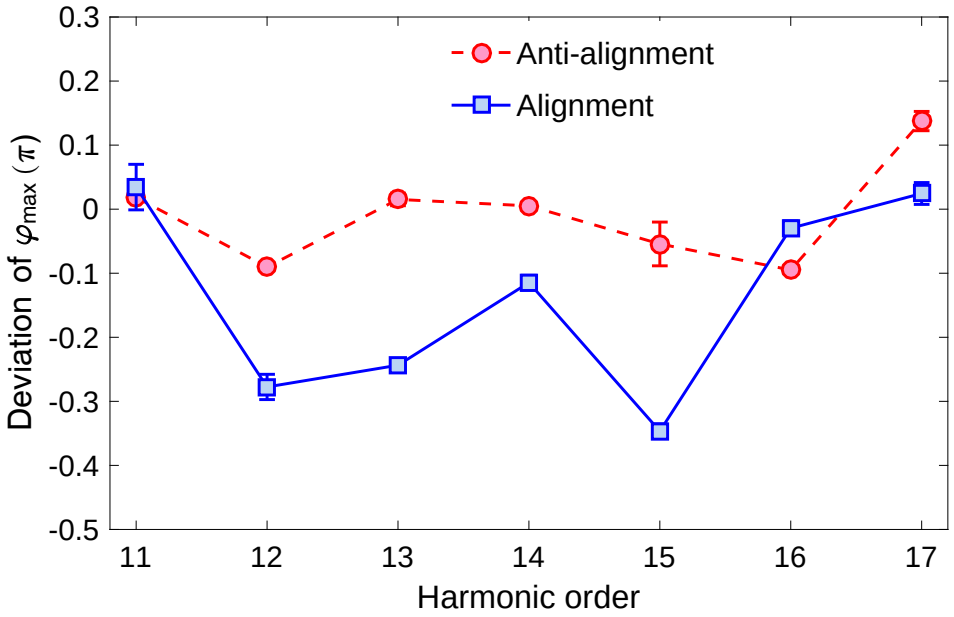

Fig S10 Deviations between the experimental extractions and single-active electron (XX channel) calculations of φ_{max} for the alignment (blue squares) and anti-alignment (red circles) of C_4H_2 molecule.

calculations of the relavtive phase $\Delta\phi_{XA}$ between $\tilde{X}$ and $\tilde{A}$ states as a function of time for both the 0° (dashed line) and 90° (solid line) alignment in Fig. S9. As shown in Fig. S9, for the 90° alignment (field-free CM), $\Delta\phi_{XA}$ increases linearly with time. The slope of the increase just corresponds to enegry gap between the $\tilde{X}$ and $\tilde{A}$ states. While for the 0° alignemnt, the laser-induced coupling between the two states gives rise to a much faster increase of $\Delta\phi_{XA}$. This is equivalent to a larger energy gap between the $\tilde{X}$ and $\tilde{A}$ states, thus corresponding to a much faster charge oscillation.

Finally, we demonstrate that the different CM dynamics along the parallel and perpendicular orientations of C_4H_2 can also be identified from our two-color HHG measurements. It has been reported that the deviation of the experimentally extracted optimal two-color relative phases φ_{max} (where the HHG intensity reaches a maximum) with respect to the single channel calculations will be an indicator for the multichannel (CM) dynamics in the molecules.[54] In Fig. S10, we have extracted φ_{max} from our two-color experiment at both the alignment and anti-alignment of C_4H_2,

and compared the results to the single XX channel calculations. In our calculations, the single XX contribution is simulated with the QRS theory. As shown in Fig. S10, the deviations of φ_{max} with respect to the single-active electron response are different between the two alignment cases. This difference provides direct experimental evidence of the different CM dynamics along these two orientations.